A Section 508–conformant HTML version of this article is available at https://doi.org/10.1289/EHP5260.

Developmental Toxicity Assessment of Piperonyl Butoxide Exposure Targeting Sonic Hedgehog Signaling and Forebrain and Face Morphogenesis in the Mouse: An *in Vitro* and *in Vivo* Study

Joshua L. Everson,[1,2] Miranda R. Sun,[1] Dustin M. Fink,[1] Galen W. Heyne,[1] Cal G. Melberg,[1] Kia F. Nelson,[1] Padydeh Doroodchi,[1] Lydia J. Colopy,[1] Caden M. Ulschmid,[1] Alexander A. Martin,[1] Matthew T. McLaughlin,[1] and Robert J. Lipinski[1,2]

[1]Department of Comparative Biosciences, School of Veterinary Medicine, University of Wisconsin-Madison, Madison, Wisconsin, USA
[2]Molecular and Environmental Toxicology Center, University of Wisconsin-Madison, Madison, Wisconsin, USA

Background: Piperonyl butoxide (PBO) is a pesticide synergist used in residential, commercial, and agricultural settings. PBO was recently found to inhibit Sonic hedgehog (Shh) signaling, a key developmental regulatory pathway. Disruption of Shh signaling is linked to birth defects, including holoprosencephaly (HPE), a malformation of the forebrain and face thought to result from complex gene–environment interactions.

Objectives: The impact of PBO on Shh signaling *in vitro* and forebrain and face development *in vivo* was examined.

Methods: The influence of PBO on Shh pathway transduction was assayed in mouse and human cell lines. To examine its teratogenic potential, a single dose of PBO (22–1,800 mg/kg) was administered by oral gavage to C57BL/6J mice at gestational day 7.75, targeting the critical period for HPE. Gene–environment interactions were investigated using $Shh^{+/-}$ mice, which model human HPE-associated genetic mutations.

Results: PBO attenuated Shh signaling *in vitro* through a mechanism similar to that of the known teratogen cyclopamine. *In utero* PBO exposure caused characteristic HPE facial dysmorphology including dose-dependent midface hypoplasia and hypotelorism, with a lowest observable effect level of 67 mg/kg. Median forebrain deficiency characteristic of HPE was observed in severely affected animals, whereas all effective doses disrupted development of Shh-dependent transient forebrain structures that generate cortical interneurons. Normally silent heterozygous *Shh* null mutations exacerbated PBO teratogenicity at all doses tested, including 33 mg/kg.

Discussion: These findings demonstrate that prenatal PBO exposure can cause overt forebrain and face malformations or neurodevelopmental disruptions with subtle or no craniofacial dysmorphology in mice. By targeting Shh signaling as a sensitive mechanism of action and examining gene–environment interactions, this study defined a lowest observable effect level for PBO developmental toxicity in mice more than 30-fold lower than previously recognized. Human exposure to PBO and its potential contribution to etiologically complex birth defects should be rigorously examined. https://doi.org/10.1289/EHP5260

Introduction

Piperonyl butoxide (PBO) is a semisynthetic pesticide synergist that inhibits insect cytochrome p450 enzyme activity (U.S. EPA 2006; Scott 1996). Most commonly used in pyrethrin- and pyrethroid-based pesticide formulas, PBO is present in hundreds of products used in agricultural, commercial, and residential settings, including indoor and outdoor foggers and topical medications like lice shampoo. These products typically contain substantially higher concentrations of PBO than the active insecticidal ingredient (U.S. EPA 2006). PBO was one of the top 10 chemical contaminants found in indoor dust sampled from 119 homes in Cape Cod, Massachusetts (Rudel et al. 2003), and was detected in 75% of personal air samples of 230 pregnant women in New York City, New York, who self-identified as either African American or Dominican (Horton et al. 2011). Use of pyrethrin- and pyrethroid-based formulations containing PBO has increased with the decline of organophosphate pesticides, as reviewed in the U.S. Environmental Protection Agency (EPA) Registration Eligibility Decision for PBO (U.S. EPA 2006). Relative to active pesticidal components, the developmental toxicity of PBO has received little research attention.

PBO was recently discovered to inhibit the Sonic hedgehog (Shh) signaling pathway in a study using high-throughput *in vitro* screening and Shh-responsive cell-based and zebrafish assays (Wang et al. 2012). The Shh pathway is required for multiple aspects of embryonic development, including morphogenesis of the forebrain and midface, as illustrated by major malformations observed in *Shh* knockout mice (Chiang et al. 1996). Shh pathway inhibition is classically associated with holoprosencephaly (HPE), a congenital condition defined by median forebrain deficiency, typically occurring with characteristic facial dysmorphology, including hypotelorism and midface hypoplasia (Weiss et al. 2018). Mice with homozygous *Shh* null mutations exhibit severe HPE (Chiang et al. 1996), and *SHH* mutations have been identified as among the most common human HPE-associated gene mutations (Nanni et al. 1999; Roessler et al. 1996, 2018; Roessler and Muenke 2010). The Shh pathway also appears to be inherently sensitive to small molecule modulation (Chen et al. 2002b; Chen 2016). Well-characterized and structurally diverse pathway antagonists include the plant alkaloid cyclopamine, which was found to cause HPE in livestock, rabbits, and rodents (Keeler 1970, 1975, 1978), and the U.S. Federal Drug Administration (FDA)-approved drug vismodegib, which was shown to cause HPE in mice (Heyne et al. 2015a, 2016).

Human HPE is an etiologically heterogeneous condition associated with significant morbidity. Although occurring in approximately 1 in 10,000 live births (Leoncini et al. 2008), HPE was estimated to have a prevalence of 1 in 250 conceptuses (Matsunaga and Shiota 1977). These observations suggest that HPE is one of the most common human developmental abnormalities, but the vast majority of affected embryos do not survive to birth. In surviving patients, HPE can cause severe intellectual disability and

Address correspondence to Robert J. Lipinski, Department of Comparative Biosciences, School of Veterinary Medicine, University of Wisconsin-Madison, 2015 Linden Dr., Madison, WI 53706 USA. Telephone: (608) 265-4043. Email: Robert.lipinski@wisc.edu

Supplemental Material is available online (https://doi.org/10.1289/EHP5260).

The authors declare they have no actual or potential competing financial interests.

Received 27 February 2019; Revised 26 July 2019; Accepted 27 September 2019; Published 23 October 2019.

Note to readers with disabilities: *EHP* strives to ensure that all journal content is accessible to all readers. However, some figures and Supplemental Material published in *EHP* articles may not conform to 508 standards due to the complexity of the information being presented. If you need assistance accessing journal content, please contact ehponline@niehs.nih.gov. Our staff will work with you to assess and meet your accessibility needs within 3 working days.

learning, behavior, and motor impairment (Levey et al. 2010; Weiss et al. 2018).

HPE is thought to arise from complex gene–environment interactions (Graham and Shaw 2005; Hong and Krauss 2018; Krauss and Hong 2016; Lovely et al. 2017; Petryk et al. 2015; Roessler et al. 2003, 2018). Most single-gene mutations linked to HPE pathogenesis have been found to be heterozygous and associated with highly variable phenotypic outcomes (Roessler and Muenke 2010). Only 25% of patients with nonchromosomal HPE have been found to have mutations in one of the four most common HPE genes (Roessler and Muenke 2010), and documented examples of clear gene–gene interactions have been exceedingly rare in humans (Roessler et al. 2018). Therefore, the environmental contribution to HPE etiology is likely substantial. However, relative to genetic factors, examination of environmental influences in the complex etiology of HPE has been largely neglected. A logical focus of such investigation is common environmental chemicals that perturb the Shh signaling pathway.

The few existing studies of the potential developmental toxicity of PBO were conducted before its inhibitory action on the Shh pathway was known and were therefore untargeted (U.S. EPA 2006). Unlike previous investigations, the studies reported here were designed to specifically examine the impact of PBO on Shh signaling. First, *in vitro* assays were used to define the impact of PBO on the Shh pathway transduction. Then, the *in vivo* developmental toxicity of PBO was tested by targeting exposure to a critical period of forebrain and face development, incorporating a clinically relevant genetic cofactor, and rigorously examining Shh-dependent outcomes.

Materials and Methods

Materials

Biologically active materials used for *in vitro* and/or *in vivo* studies included recombinant human SHH ligand (Catalog No. 1845-SH; R&D Systems), vismodegib (Catalog No. V-4050; LC Labs), cyclopamine (Catalog No. C-8700; LC Labs), the Smoothened (SMO) agonist (SAG; Catalog No. S7779; Selleckchem), and PBO (Catalog No. P490200; Toronto Research Chemicals). The supplier-stated purity of PBO was >96% and our own liquid chromatography–mass spectrometry analysis suggested a purity of 98.11%, with the presence of four minor impurities (see Figure S1).

In Vitro *Cell Culture*

Mammalian cell culture assays were used to evaluate the impact of PBO on Shh signaling. Most assays utilized mouse embryonic fibroblasts (MEFs) that recapitulate Shh-responsiveness during embryonic development (Lipinski et al. 2006, 2008). MEF lines examined included SHH LightII-3T3 MEFs expressing a GLI-driven firefly luciferase and constitutive renilla luciferase (Taipale et al. 2000), *Ptch1*$^{-/-}$ MEFs (Taipale et al. 2000), and MEFs overexpressing *GLI1* (*GLI1* OE) (Lipinski et al. 2008) or *SMO*^{M2} (*SMO*^{M2} OE; previously indicated as Smo*) (Lipinski et al. 2008). Mouse cell lines were grown in Dulbecco's Modified Eagle Medium (DMEM) with L-glutamine, 4.5 g/L D-glucose without sodium pyruvate (Catalog No. 10-017-CV; Corning Life Sciences) with 10% fetal bovine serum (FBS; Catalog No. SH30071.03; GE Healthcare Life Sciences), and 1% penicillin-streptomycin (pen-strep) and subcultured 1:5 to 1:10 for maintenance. Human Shh subgroup medulloblastoma (DAOY) cells (Jacobsen et al. 1985) were purchased (Catalog No. HTB-186; ATCC) and grown in Eagle's Minimum Essential Medium (EMEM; Catalog No. 30-2003; ATCC) with 10% FBS and 1% pen-strep and subcultured 1:5 for maintenance. For treatment, all cells were plated at 5×10^5 cells/mL (0.4 mL per well in a 24-well plate) and allowed to attach in complete medium for 24 h before media were replaced with DMEM or EMEM containing 1% FBS ± recombinant human SHH ligand (0.4 μg/mL final concentration), made in a stock solution at 100 μg/mL in sterile-filtered 5 mg/mL bovine serum albumin (BSA) in phosphate buffered saline (PBS), vismodegib [in dimethyl sulfoxide (DMSO)], cyclopamine (in DMSO), PBO (in DMSO), and/or SAG (in water). For concentration–response assays in SHH LightII-3T3 cells, serial dilutions were prepared to achieve the following concentrations: PBO at 4.11 nM, 12.3 nM, 37.0 nM, 111.1 nM, 333.3 nM, 1.0 μM, 3.0 μM, 9.0 μM, and 27.0 μM; cyclopamine at 0.457 nM, 1.37 nM, 4.11 nM, 12.3 nM, 37.0 nM, 111.1 nM, 333.3 nM, 1.0 μM, and 3.0 μM; vismodegib at 0.0508 nM, 0.152 nM, 0.457 nM, 1.37 nM, 4.11 nM, 12.3 nM, 37.0 nM, and 111.1 nM. Concentration ranges were established by pilot range-finding experiments. One-hundred percent DMSO was added to each well at a volume to equal the DMSO concentration of the highest concentration of each drug. Control cells were treated with equivalent volumes of 5 mg/mL BSA and/or 100% DMSO. For experiments using *Ptch1*$^{-/-}$, *SMO*^{M2} OE, and *GLI1* OE cell lines, serial dilutions of PBO were prepared to achieve concentrations of 0.45 μM, 1.35 μM, and 4.05 μM. One-hundred percent DMSO was added to each well at a volume to equal the DMSO concentration of the highest concentration of PBO. For co-exposure experiments, *Ptch1*$^{-/-}$ cells were treated with 2 μM PBO ± 50.0 nM SAG. Control cells were treated with equivalent volumes of 100% DMSO. After 48 h, cells were harvested for luciferase assays or RNA isolation.

Luciferase Assays

After media were removed, SHH LightII-3T3 MEF cells were washed once in PBS. Then lysates were collected in Passive Lysis Buffer (Catalog No. E1941; Promega) and luciferase activity was assayed using the Dual-Luciferase® Reporter Assay System (Catalog No. E1910; Promega) according to manufacturer specifications. Relative light units (RLUs) for Firefly and Renilla luciferase were generated using a TD-20/20 luminometer (Catalog No. 2020-998; Turner Designs). The difference between SHH- and vehicle-treatment groups was used as a baseline to calculate the effect of drug exposure on relative GLI-dependent luciferase activity. Percentage reduction from SHH-treated values shown in Figure 1B were calculated for each experimental drug concentration treatment group (x) using the following equation:

$$\text{Percentage reduction from SHH treated} = \frac{\text{SHH}_{\text{Ctl}} - x}{\text{SHH}_{\text{Ctl}} - \text{Veh}_{\text{Ctl}}} \times 100,$$

where SHH_{Ctl} = relative luciferase of SHH + DMSO; Veh_{Ctl} = relative luciferase of DMSO; and x = relative luciferase of SHH + drug at the given concentration. Calculations used SHH_{Ctl} and Veh_{Ctl} values generated within the same biological replicate experiment. Percentage reduction from SHH-treated values were used to establish concentration–response curves and approximate half maximal effective concentration (EC_{50}) values using Graphpad Prism (version 7; GraphPad Software Inc.).

Gene Expression Analysis of in Vitro *Assays*

For *in vitro* samples, cells were washed once in PBS before RNA isolation using GE Illustra RNAspin kits (Catalog No. 25-0500-72; GE Healthcare Life Sciences) according to manufacturer recommendations. Eluted RNA was stored at −80°C. Complementary

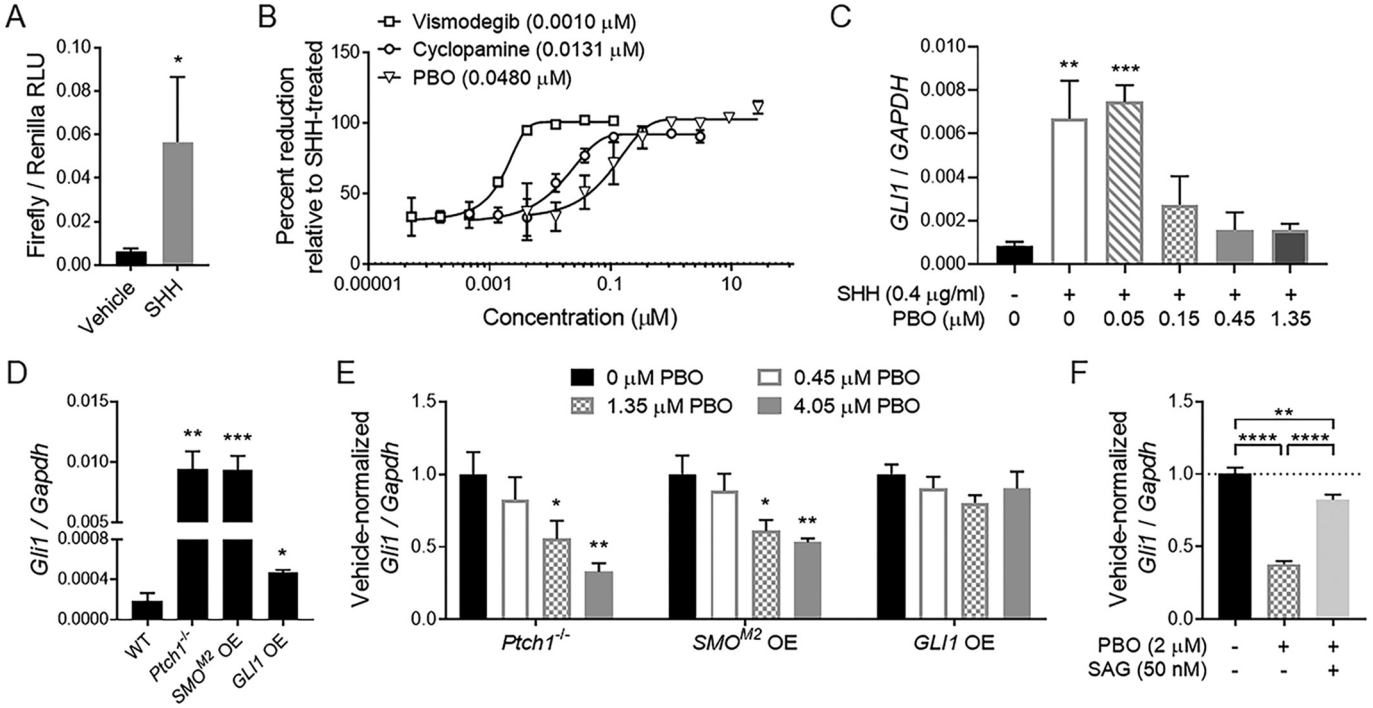

Figure 1. Shh signaling activity in PBO-treated mouse and human cells. SHH LightII-3T3 MEFs were treated ±0.4 μg/mL SHH ligand and ±graded concentrations of PBO, cyclopamine, or vismodegib. Cells were harvested after 48 h and GLI-responsive firefly luciferase was measured and normalized to renilla luciferase activity. (A) Firefly luciferase activity in cells treated with SHH or vehicle (DMSO). Values represent the mean ± SE of four biological replicate experiments. A two-tailed *t*-test with Holm-Sidak correction was used to compare the statistical significance of relative luciferase activity between SHH- and vehicle-treatment groups. $^{*}p<0.05$. (B) The difference between SHH- and vehicle-treatment groups was used as a baseline to determine the effect of drug exposure, calculated as percentage reduction in luciferase activity relative to SHH treatment alone. These values were used to establish concentration–response curves and approximate half maximal effective concentration (EC_{50}) values for each drug listed in parentheses. Values represent the mean ± SE of four biological replicate experiments. (C) Human medulloblastoma (DAOY) cells were treated ±0.4 μg/mL SHH ligand and indicated concentrations of PBO, and *GLI1* relative to *GAPDH* expression was measured. Values represent the mean ± SE of four biological replicate experiments. A one-way ANOVA followed by two-tailed *t*-tests with Holm-Sidak correction were used to compare the statistical significance of SHH ± PBO-treated groups against the control (DMSO) group. $^{**}p<0.01$; $^{***}p<0.001$. (D) Baseline Shh pathway activity in $Ptch1^{-/-}$ MEFs and those overexpressing (OE) either SMO^{M2} or *GLI1* was compared with that in WT MEFs by examining *Gli1* relative to *Gapdh* expression. Values represent the mean ± SE of five biological replicate experiments. Two-tailed *t*-tests with Welch's correction were used to compare statistical significance of relative *Gli1* expression in $Ptch1^{-/-}$ MEFs, SMO^{M2} OE MEFs, and *GLI1* OE MEFs against relative *Gli1* expression in WT MEFs. $^{*}p<0.05$; $^{**}p<0.01$; $^{***}p<0.001$. (E) $Ptch1^{-/-}$, SMO^{M2} OE, or *GLI1* OE cells were treated ±the indicated PBO concentrations, and *Gli1* relative to *Gapdh* expression was measured. Values from individual biological replicate experiments were normalized to the vehicle control group to show comparable fold changes. Values represent the mean ± SE of six biological replicate experiments. A one-way ANOVA followed by two-tailed *t*-tests with Holm-Sidak correction were used to compare the statistical significance of PBO-treated groups against the control (DMSO) group. $^{*}p<0.05$; $^{**}p<0.01$. (F) $Ptch1^{-/-}$ MEFs were treated ±2 μM PBO and ±50 nM SMO agonist SAG. Values from individual biological replicates were normalized to the vehicle (DMSO) control group. Values represent the mean ± SE of four biological replicate experiments. One-way ANOVA followed by two-tailed *t*-tests with Holm-Sidak correction were used to compare the statistical significance between the vehicle and PBO ± SAG treated groups. $^{**}p<0.01$; $^{****}p<0.0001$. Note: DMSO, dimethyl sulfoxide; MEFs, mouse embryonic fibroblasts; PBO, piperonyl butoxide; RLU, relative luciferase activity; SAG, Smoothened agonist; SE, standard error; SHH, Sonic hedgehog ligand; SMO, Smoothened; WT, wild type.

DNA (cDNA) was synthesized from 250 ng of total RNA using GoScript reverse transcription reaction kits (Catalog No. A2791; Promega). Singleplex quantitative real-time polymerase chain reaction (qRT-PCR) was performed using a Bio-Rad CFX96 real-time PCR detection system (Bio-Rad Laboratories). The reaction mixture contained 0.75 μL cDNA, 6 μL SSoFast EvaGreen Supermix (Catalog No. 1725201; Bio-Rad Laboratories), 4.75 μL nuclease-free water, and 0.5 μL of 10 μM forward and reverse gene-specific primers designed using the IDT PrimerQuest tool (Integrated DNA Technologies). qRT-PCR primer sequences are listed in Table S1. Target gene specificity was confirmed using National Center for Biotechnology Information Primer-Basic Local Alignment Search Tool (NCBI Primer-BLAST). The gene glyceraldehyde-3-phosphate dehydrogenase (*Gapdh*) (mouse) or *GAPDH* (human) was used as the housekeeping gene, and analyses were conducted with the 2^{-ddCt} method. qRT-PCR conditions were as follows: one cycle at 95°C for 3 min, then 40 cycles × at 95°C for 10 s followed by 60°C for 30 s.

Animal Husbandry

This study was conducted in strict accordance with the recommendations in the *Guide for the Care and Use of Laboratory Animals* of the National Institutes of Health (NIH) (NRC 2011). The protocol was approved by the University of Wisconsin School of Veterinary Medicine Institutional Animal Care and Use Committee (Protocol No. 13–081.0). Mice harboring the *Shh* null allele as described by Chiang et al. (1996) were provided by Dr. Philip Beachy and backcrossed to the C57BL/6J background for more than 15 generations. Male and female C57BL/6J mice (Strain No. 00664; Jackson Laboratory) were housed under specific-pathogen-free conditions in disposable, ventilated cages (Innovive). Rooms were maintained at 22 ± 2°C and 30–70% humidity on a 12-h light, 12-h dark cycle. Mice were fed Irradiated Soy Protein-Free Extruded Rodent Diet (Catalog No. 2920x; Envigo Teklad Global) until day of plug, when dams received Irradiated Teklad Global 19% Protein Extruded Rodent Diet (Catalog No. 2919; Envigo Teklad Global).

Table 1. Descriptors of the WT study population shown in Figure 2.

Treatment (dose)	Litters collected (n)	Live fetuses [n (mean)]	Resorptions [n (mean)]	Crown–rump [(mean ± SD) mm]
Vehicle	11	66 (6.0)	5 (0.45)	16.74 ± 0.85
PBO (22.22 mg/kg)	3	22 (7.3)	1 (0.33)	16.73 ± 0.88
PBO (66.67 mg/kg)	4	26 (6.5)	4 (1.00)	16.83 ± 0.58
PBO (200 mg/kg)	6	45 (7.5)	3 (0.50)	16.61 ± 0.87
PBO (600 mg/kg)	5	39 (7.8)	3 (0.60)	16.35 ± 0.86
PBO (1,800 mg/kg)	5	25 (5.0)	13 (2.60)[a]	16.32 ± 0.88

Note: Timed-pregnant C57BL/6J mice were administered the indicated doses of piperonyl butoxide (PBO) at gestational day (GD)7.75 and inspected at GD17 for live fetuses and resorptions. One-way ANOVA was used to compare number of live fetuses, resorptions, and crown–rump lengths between vehicle- and PBO-treated groups. No statistically significant differences were detected. PBO, piperonyl butoxide; SD, standard deviation; WT, wild type.
[a]Includes two litters with early resorbing embryos that were difficult to individually distinguish.

General Animal Study Design

One to two nulliparous female C57BL/6J wild-type (WT) mice were placed with a single C57BL/6J WT or *Shh*$^{+/-}$ male for 1–2 h and subsequently examined for the presence of copulation plugs. The beginning of the mating period was designated as gestational day (GD)0. Pregnancy was confirmed by assessing weight gain at GD7, as previously described (Heyne et al. 2015b). Timed-pregnant dams were administered PBO dissolved in reagent-grade olive oil (Catalog No. OL130; Spectrum Chemical), vehicle (olive oil alone), or vismodegib (as a positive control) by oral gavage at GD7.75 ± 20 min. Vismodegib was suspended in 0.5% methyl cellulose with 0.2% Tween-80 as previously described (Heyne et al. 2015a, 2016). Pregnant dams were euthanized by carbon dioxide inhalation followed by cervical dislocation at GD8.25 ± 1 h or GD11 ± 1 h for embryo collection or at GD17 ± 2 h for fetal collection. Animal husbandry, drug administration, and embryo/fetal collection were conducted by individuals not blinded to experimental condition.

Facial Morphometric Analysis

For quantitative assessment of fetal facial morphology, WT dams were administered vehicle ($n = 11$) or 22.22 ($n = 3$), 66.67 ($n = 4$), 200 ($n = 6$), 600 ($n = 5$), or 1,800 mg/kg PBO ($n = 5$). Following euthanasia at GD17, dam uteri were inspected for resorptions and live fetuses, and crown–rump length was recorded for each fetus. Population parameters for the WT mouse study arm are described in Table 1. To assess gene–environment interactions, WT female mice mated with *Shh*$^{+/-}$ male mice were administered vehicle ($n = 7$) or 33 ($n = 6$), 110 ($n = 7$), or 300 mg/kg PBO ($n = 7$). Following euthanasia at GD17, dam uteri were inspected for resorptions and live fetuses, and crown–rump length was recorded for each fetus. Population parameters for the study arm using *Shh*$^{+/+}$ and *Shh*$^{+/-}$ mice are described in Table 2. Interdigitated doses of PBO were chosen for these separate study arms to maximize dose–response data and avoid experimental duplication. For both study arms, all viable fetuses collected from each litter were included in the facial morphometric analyses. Fetuses were fixed in 10% phosphate buffered formalin and imaged by light microscopy, with careful attention placed on consistent positioning of the head and face. Light microscopic images of GD17 fetuses were captured using a MicroPublisher 5.0 camera (QImaging) connected to an SZX-10 stereomicroscope (Olympus). Interocular distance (IOD) and upper lip length (ULL) measurements were made from images using ImageJ (Schneider et al. 2012) by a single rater blinded to genotype and treatment group.

Analysis of Embryonic Morphology

For qualitative assessment of embryonic face and brain morphology, embryos exposed to vehicle or 1,800 mg/kg PBO were collected at GD11. For each treatment group, two to three litters were collected and fixed in 4% paraformaldehyde (PFA) overnight, then dehydrated into methanol and stored at −20°C. Following rehydration into PBS, representative embryos were imaged using a QImaging MicroPublisher 5.0 camera connected to an Olympus SZX-10 stereomicroscope.

Analysis of Fetal Face and Brain Morphology

For qualitative assessment of correlative face and brain morphology, litters exposed to vehicle; 200, 600, or 1,800 mg/kg PBO; or 40 mg/kg vismodegib were collected at GD17 and fixed in Bouin's solution. Single litters were generated for each treatment group. From each litter, fetuses with facial dysmorphology representative of the corresponding group in the larger WT population were selected for histological analysis. Following paraffin embedding, 10-μm sections were produced and stained with hematoxylin and eosin (H&E) by standard protocols. Light microscopic images of fetal faces (before or after Bouin's fixation) and histological sections were captured using a QImaging MicroPublisher 5.0 camera connected to an Olympus SZX-10 stereomicroscope.

Medial Ganglionic Eminence Morphometric Analysis

For quantitative assessment of medial ganglionic eminence (MGE) morphology, WT litters exposed to vehicle ($n = 5$) or 22.22 ($n = 3$), 66.67 ($n = 3$), 200 ($n = 3$), or 600 mg/kg PBO ($n = 3$) were collected at GD11. Embryos were fixed in 4% PFA overnight, then dehydrated into methanol and stored at −20°C. Embryos were then rehydrated into PBS, hemisected sagittally using a scalpel, and imaged by light microscopy using a

Table 2. Descriptors of the gene–environment study population shown in Figure 4.

Treatment (dose)	Litters collected (n)	Live fetuses [n (mean)]	Resorptions [n (mean)]	*Shh*$^{+/+}$ fetuses (n)	*Shh*$^{+/-}$ fetuses (n)	*Shh*$^{+/+}$ mean crown–rump ± SD (mm)	*Shh*$^{+/-}$ mean crown–rump ± SD (mm)
Vehicle	7	48 (6.8)	3 (0.43)	26	22	16.54 ± 0.88	16.30 ± 0.78
PBO (33 mg/kg)	6	39 (6.5)	4 (0.67)	21	18	16.62 ± 0.61	16.25 ± 0.67
PBO (100 mg/kg)	7	42 (6.0)	9 (1.29)	22	20	16.73 ± 1.22	16.13 ± 0.97
PBO (300 mg/kg)	7	48 (6.8)	2 (0.28)	24	24	16.23 ± 0.53	16.24 ± 0.89

Note: WT C57BL/6J female mice were mated with *Shh*$^{+/-}$ male mice and administered the indicated doses of piperonyl butoxide (PBO) at gestational day (GD)7.75. At GD17, dams were inspected for live fetuses and resorptions, and fetuses were genotyped. One-way ANOVA was used to compare number of live fetuses, resorptions, and crown–rump lengths between vehicle- and PBO-treated groups of *Shh*$^{+/+}$ and *Shh*$^{+/-}$ fetuses. No statistically significant differences were detected. ANOVA, analysis of variance; Shh, Sonic hedgehog; SD, standard deviation; WT, wild type.

QImaging MicroPublisher 5.0 camera connected to an Olympus SZX-10 stereomicroscope. Area measurements of the MGEs and head were made in ImageJ. Measurements were made by a single rater blinded to treatment group.

Embryonic Gene Expression Analysis

For gene expression analysis, vehicle-exposed ($n=5$) and 1,800 mg/kg PBO-exposed litters ($n=4$) were collected at GD8.25. Somites were counted (Theiler 1989) and from all embryos with 7–10 somites anterior neural folds were isolated by microdissection in cold PBS. Isolated neural fold tissue was pooled for each litter and frozen immediately on dry ice. RNA was isolated using GE Illustra RNAspin kits (Catalog No. 25-0500-72; GE Healthcare Life Sciences) and stored at −80°C. cDNA was synthesized from 250 ng of total RNA using GoScript reverse transcription reaction kits (Catalog No. A2791; Promega). Singleplex qRT-PCR was performed using a Bio-Rad CFX96 real-time PCR detection system (Bio-Rad Laboratories) as described above for gene expression analysis of *in vitro* samples.

In Situ *Hybridization and Riboprobe Synthesis*

Riboprobes were synthesized by PCR as previously described (Abler et al. 2011). Briefly, sequence-specific cDNA was first amplified and affixed with a 3′ T7 RNA-polymerase recognition site using a Taq DNA-polymerase kit (Catalog No. 201203; Qiagen), GD12 whole-embryo cDNA as a template, and primers targeting *Gli1* [forward-CCCTCCTCCTCTCATTCCAC and reverse-*CGATGTTAATACGACTCACTATAGGG*TCCAGCTGA-GTGTTGTCCAG (italicized nucleotides denote the T7-polymerase recognition site and a 5-bp spacer sequence)]. Gene-specific primers were designed using the IDT PrimerQuest tool, and sequence specificity was confirmed using NCBI Primer-BLAST. Following PCR, *Gli1*-amplified cDNA was recovered by gel extraction using an E. Z.N.A. Gel Extraction Kit (Catalog No. D2500-01; Omega Bio-Tek). Next, digoxygenen-11-uridine-5′-triphosphate (UTP)-labeled riboprobes were synthesized from the *Gli1* cDNA template using T7 RNA-polymerase (Catalog No. P2075; Promega) in the presence of Digoxygenin-labeled UTPs (Catalog No. 11277073910; Roche Life Science). Last, riboprobes were purified using Illustra RNAspin kits (Catalog No. 25-0500-72; GE Healthcare Life Sciences) and stored at −80°C. *In situ* hybridization (ISH) was then conducted to visualize *Gli1* expression, as previously described (Abler et al. 2011), but omitting the proteinase K/collagenase step. Anti-digoxygenin alkaline phosphatase-conjugated antibodies (Catalog No. 11093274910; Roche Life Science) were used to target the riboprobe *in situ*, and samples were then incubated with BM-Purple (Catalog No. 11442074001; Roche Life Science) to generate a blue colorimetric stain visible by light microscopy. Embryos images were captured using a QImaging MicroPublisher 5.0 camera connected to an Olympus SZX-10 stereomicroscope.

Statistics

Graphpad Prism 7 was used for all statistical analyses. One-way analysis of variance (ANOVA) with Tukey's post hoc test for multiple comparisons was used for analyses of linear facial measurements, MGE area measurements, litter sizes, and crown–rump lengths. One-way ANOVA followed by two-tailed *t*-tests with Holm-Sidak correction were used to determine whether gene expression was changed by the treatment condition *in vivo*, in DAOY cells, SHH LightII-3T3 MEFs, *Ptch1*$^{-/-}$ MEFs, *SMO*^{M2} OE MEFs, and *GLI1* OE MEFs, and for *Ptch1*$^{-/-}$ SAG rescue experiments. Two-tailed *t*-tests with Welch's correction were used to determine whether basal *Gli1* expression was different in *Ptch1*$^{-/-}$ MEFs, *SMO*^{M2} OE MEFs, and *GLI1* OE MEFs compared with WT MEFs. An alpha value of 0.05 was maintained for determination of significance for all experiments.

Results

Influence of PBO on Shh Signaling Pathway Transduction in Vitro

The influence of PBO on Shh signaling pathway transduction was examined with mammalian cell culture assays that have been used previously to discover and validate structurally diverse pathway inhibitors (Chen et al. 2002a, 2002b; Lipinski and Bushman 2010). First, the concentration–response activity of PBO was tested relative to index pathway inhibitors cyclopamine and vismodegib. SHH LightII-3T3 cells were treated with recombinant human SHH ± graded concentrations of PBO, cyclopamine, vismodegib, or vehicle alone. Addition of SHH ligand resulted in significantly higher relative activity of GLI-responsive firefly luciferase compared with vehicle treatment (Figure 1A). The difference between SHH- and vehicle-treatment groups was used as a baseline to determine the effect of drug exposure, calculated as percentage reduction in luciferase activity relative to SHH treatment alone. The addition of PBO, cyclopamine, and vismodegib each resulted in lower GLI-dependent luciferase activity in a manner that appeared concentration dependent (Figure 1B). These values were used to establish concentration–response curves and approximate EC_{50} values for each drug (Figure 1B). Next, the effect of PBO on Shh signaling in human cells was examined in a Shh subgroup medulloblastoma (DAOY) cell line. DAOY cells were treated with SHH ligand ± graded concentrations of PBO or vehicle alone, and expression of the conserved Shh pathway gene *GLI1* was measured relative to *GAPDH*. Addition of SHH ligand resulted in significantly higher *GLI1* expression compared with the vehicle treatment (Figure 1C). Compared with SHH treatment alone, addition of PBO resulted in lower *GLI1* expression in a manner that appeared concentration dependent. No differences were observed in expression of the HPE-associated genes Bone morphogenetic protein 4 (*BMP4*) or SIX Homeobox 3 (*SIX3*) in response to SHH or PBO treatment (see Figure S2).

Normally, SHH ligand binding to the Patched (PTCH1) receptor relieves its inhibition of SMO (Taipale et al. 2002), triggering downstream signal transduction that culminates in target gene regulation by the GLI transcription factors (Lipinski et al. 2006). Cyclopamine and vismodegib inhibit Shh signaling by directly binding to SMO (Chen et al. 2002a; Robarge et al. 2009). Cell lines with constitutive Shh pathway activity driven by genetic alterations at three unique signal transduction steps were utilized to examine the mechanism by which PBO impacts Shh signaling. Compared with WT cells, both *Ptch1* null cells and WT cells expressing *SMO*^{M2} (a constitutively active form of *SMO*) or *GLI1* exhibited higher expression levels of the conserved Shh pathway target gene *Gli1* (Figure 1D). In both *Ptch1* null cells and WT cells expressing *SMO*^{M2}, PBO treatment resulted in lower *Gli1* expression in a manner that appeared concentration dependent (Figure 1E). In cells with *GLI1* overexpression driving pathway activity downstream of SMO, no difference in *Gli1* expression was observed between the PBO- and vehicle-treatment groups. Finally, in *Ptch1* null cells, we found that reduced *Gli1* expression resulting from PBO exposure was partially rescued by the addition of SAG (Figure 1F).

In Vivo *Teratogenicity*

Next, the teratogenic potential of PBO was examined by administering PBO acutely to timed-pregnant C57BL/6J mice by oral gavage at GD7.75 to target the critical period for induction of

HPE (Heyne et al. 2015a; Lipinski et al. 2010). Dams were euthanized at GD17, and uteri were carefully inspected. The number of resorptions and live fetuses in each litter, as well as mean crown–rump length were calculated (Table 1). No significant differences in these values were detected in any of the treatment groups. In 2 of 5 dams administered 1,800 mg/kg PBO, only resorbed embryos were observed, resulting in a modest and not statistically significant lower average number of live fetuses per litter in this treatment group. In all other PBO-dose groups (22.22–600 mg/kg), the average number of surviving fetuses per litter was similar to that of the vehicle-exposed group.

Facial morphology was examined in GD17 fetuses by measuring ULL and IOD (Figure 2). These measurements have been used to assess midline morphogenesis and found to be useful predictors of underlying HPE-associated brain malformations (Heyne et al. 2016; Kietzman et al. 2014; Lipinski et al. 2012). Compared with the vehicle group, PBO exposure resulted in smaller IOD measurements. This appeared to be a dose-dependent effect, with a lowest observable effect level (LOEL) of 66.67 mg/kg (Figure 2G). The effect of PBO exposure on ULL was more variable, although significantly higher ULL measurements were observed in the 200 and 1,800 mg/kg PBO-exposure groups relative to the controls (Figure 2H). Increased ULL has been shown to reflect median tissue deficiency and loss of the midline upper lip notch (Lipinski et al. 2012). No other gross structural malformations in PBO-exposed fetuses were noted upon visual inspection.

Correlative Face–Brain Dysmorphology

Next, qualitative assessment of correlative face and brain dysmorphology was conducted on GD17 fetuses exposed to vehicle; 200, 600, or 1,800 mg/kg PBO; or 40 mg/kg vismodegib (as a positive control) (Figure 3). In PBO-exposed fetuses, smaller IOD and larger ULL corresponded with increasingly severe median forebrain deficiency (Figure 3B–E, 3B′–E′). Relative to vehicle-exposed controls, PBO-exposed animals with subtle facial dysmorphology exhibited smaller forebrain septal region areas (Figure 3A′–C′), whereas those with severe facial dysmorphology exhibited overt HPE, illustrated by the absence of the septal region and a single forebrain ventricle (Figure 3D′–E′). Marked telencephalic hypoplasia and olfactory bulb aplasia were also observed in severely affected PBO-exposed animals (see Figure S3). As described previously (Heyne et al. 2015a, 2016),

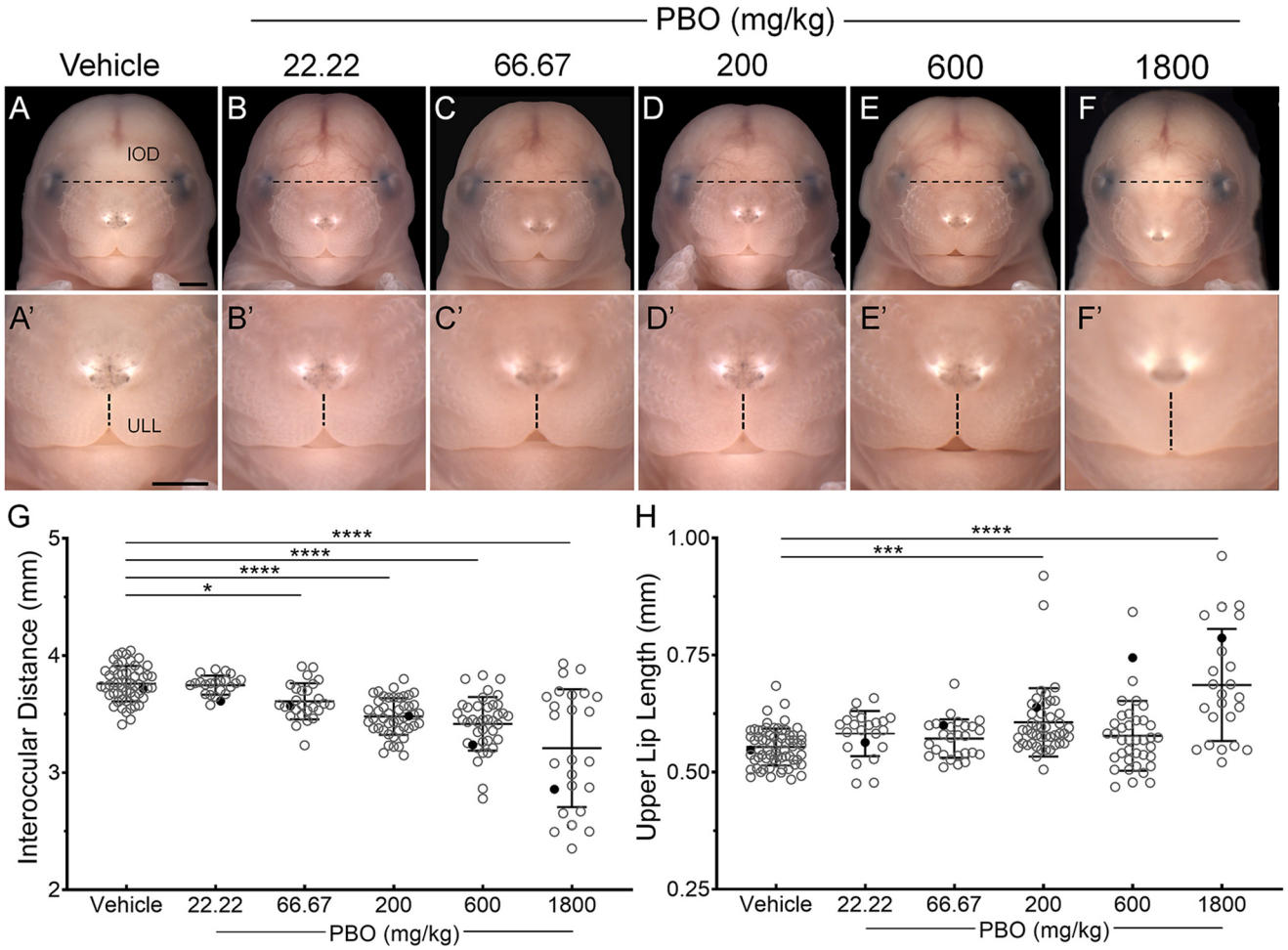

Figure 2. Evaluation of facial dysmorphology in a mouse model of targeted *in utero* PBO exposure. (A–F) GD17 fetuses exposed to vehicle (olive oil) or the indicated doses of PBO. (A′–F′) Magnified images of fetuses in A–F highlight midfacial morphology. Dashed lines in A–F mark interocular distance (IOD) shown in G, while those in A′–F′ mark upper lip length (ULL) shown in H. (G,H) Plots showing IOD and ULL measurements of fetuses exposed to vehicle ($n=66$) or 22.22 ($n=22$), 66.67 ($n=26$), 200 ($n=44$), 600 ($n=39$), or 1,800 mg/kg PBO ($n=25$). All individual data points are plotted along with bars representing the mean ± SD for each group. Filled circles in G and H indicate specific fetuses shown in A–F for the corresponding treatment group. One-way ANOVA with Tukey's post hoc test was used to compare the statistical significance of IOD and ULL measurements in PBO-exposed groups relative to the vehicle-exposed group. $^{*}p<0.05$; $^{***}p<0.001$; $^{****}p<0.0001$. Scale bars in A and A′: 1.0 mm. Note: ANOVA, analysis of variance; GD, gestational day; PBO, piperonyl butoxide; SD, standard deviation.

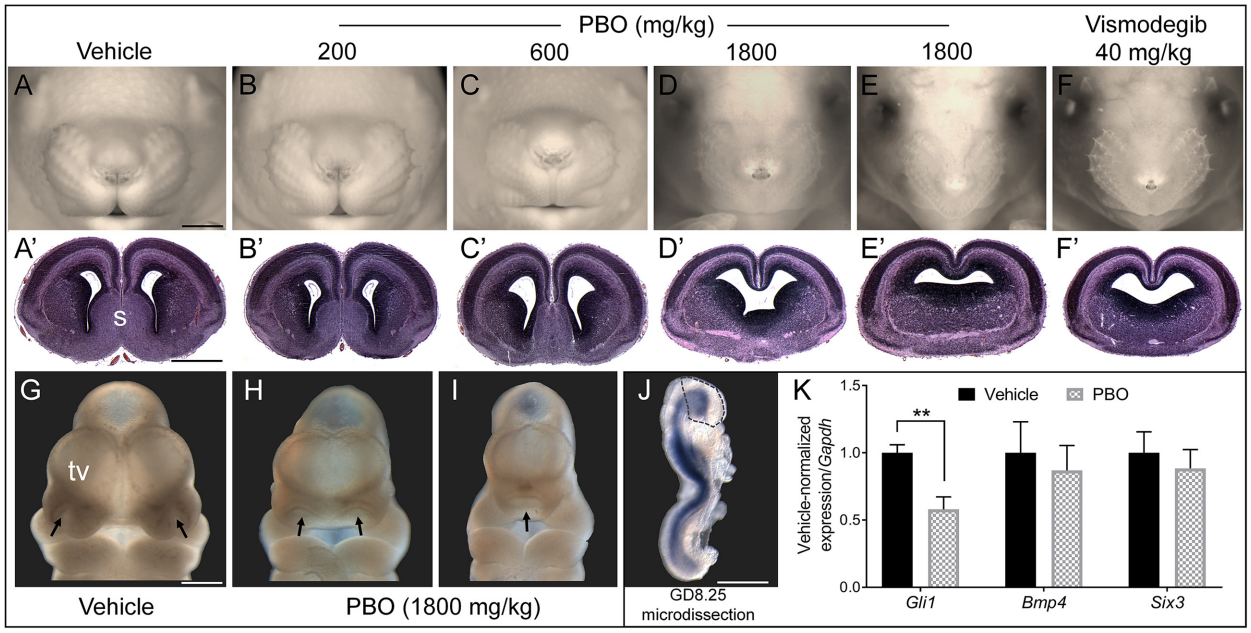

Figure 3. Assessment of corresponding face and brain morphology and *Gli1* expression in PBO-exposed embryos and fetuses. (A–F) Midfacial morphology is shown in representative GD17 fetuses exposed to vehicle (olive oil), the indicated doses of PBO, or 40 mg/kg vismodegib. Images taken before (D–F) or after fixation (A–C) show facial dysmorphology. (A′–F′) Coronal sections from mice in A–F show forebrain abnormalities co-occurring with facial dysmorphology involving the forebrain septal region(s) and lateral ventricles. (G–I) Light microscopy images of unstained representative GD11 embryos exposed to vehicle or 1,800 mg/kg PBO show abnormalities involving the telencephalic vesicles (tv) and nostrils (arrows). (J) A GD8.25 embryo stained by ISH to visualize *Gli1* expression is shown to illustrate the anterior neural fold region (dashed outline) that was microdissected from GD8.25 embryos exposed to vehicle or 1,800 mg/kg PBO. (K) Gene expression analysis by qRT-PCR of *Gli1*, *Bmp4*, and *Six3* relative to *Gapdh*. Values represent the mean ± SE of $n = 5$ vehicle-treated litters and $n = 4$ PBO-treated litters. Two-tailed *t*-tests with Holm-Sidak correction were used to compare the statistical significance of gene expression in the PBO-treatment group to the vehicle group. $^{**}p < 0.01$. Scale bars in A and A′: 1 mm, and in G and J: 0.5 mm. Note: GD, gestational day; ISH, *in situ* hybridization; PBO, piperonyl butoxide; qRT-PCR, quantitative real-time polymerase chain reaction; SE, standard error.

fetuses exposed to 40 mg/kg vismodegib exhibited overt face and forebrain dysmorphology that was characteristic of HPE and similar to that observed in overtly affected fetuses exposed to 1,800 mg/kg PBO (Figure 3F and 3F′).

The pathogenesis of PBO-induced HPE was next examined by comparing GD11 vehicle-exposed control embryos to those from dams exposed to 1,800 mg/kg PBO at GD7.75. Overt malformations of the developing face and brain were evident at GD11, with affected PBO-exposed embryos exhibiting partially or completely fused telencephalic vesicles and closely spaced or fused nostrils (Figure 3G–I). To examine the initial molecular pathogenesis of PBO-induced HPE, litters from dams exposed to vehicle or 1,800 mg/kg PBO at GD7.75 were harvested 12 h after exposure at GD8.25. Embryonic forebrain tissue was isolated by microdissection of the prosencephalic neural folds (dashed outline in Figure 3J) and harvested for mRNA. Compared with the vehicle-exposed group, PBO exposure resulted in significantly lower *Gli1* expression, but no difference in expression of the HPE-associated genes *Bmp4* and *Six3* was detected (Figure 3K).

Gene–Environment Interactions in HPE Genesis

The influence of normally silent single-allele mutations in the *Shh* gene was examined by administering PBO to timed-pregnant WT C57BL/6J female mice mated to $Shh^{+/-}$ male mice. This experimental paradigm was chosen to specifically isolate the variable of *Shh* heterozygosity. Mice harboring the *Shh* null allele were backcrossed to the C57BL/6J strain for more than 15 generations, and the mating strategy generated litters with both $Shh^{+/+}$ and $Shh^{+/-}$ embryos at equal proportion. Litters were harvested at GD17, and the number of live fetuses and resorptions, as well as mean crown–rump measurements were calculated (Table 2). No significant differences in these values were observed between dose or treatment groups. Facial morphology was examined as previously in WT trials (Figure 4A–H). No difference was observed in ULL or IOD between vehicle-exposed $Shh^{+/+}$ and $Shh^{+/-}$ fetuses (Figure 4I–J). However, at all three PBO doses (33.3, 100, or 300 mg/kg), $Shh^{+/-}$ fetuses exhibited more severe facial dysmorphology (lower IOD and higher ULL measurements) than WT fetuses (Figure 4I–J).

Subteratogenic Impact on Forebrain Development

Finally, the impact of acute prenatal PBO exposure on morphogenesis of the MGEs was examined because development of these transient forebrain structures has been shown to be Shh dependent (Kohtz et al. 1998; Xu et al. 2005). MGE morphology was examined in embryos exposed to vehicle or PBO by measuring the area of MGEs relative to total head size (Figure 5A,B). PBO exposure resulted in smaller normalized MGE areas, the size of which appeared to be PBO dose dependent with an LOEL of 66.67 mg/kg (Figure 5B–G′). Severe disruption of MGE development in the 600 mg/kg PBO-exposure group was comparable to that observed in embryos exposed to 15 mg/kg vismodegib (see Figure S4).

Discussion

Identification of environmental agents that contribute to birth defect etiology but can be avoided during pregnancy through risk communication offers a remarkably direct path to prevention. To the best of our knowledge, this report is the first to mechanistically investigate the developmental toxicity of PBO by specifically targeting the Shh signaling pathway during the critical period for HPE induction. We found that acute PBO exposure at

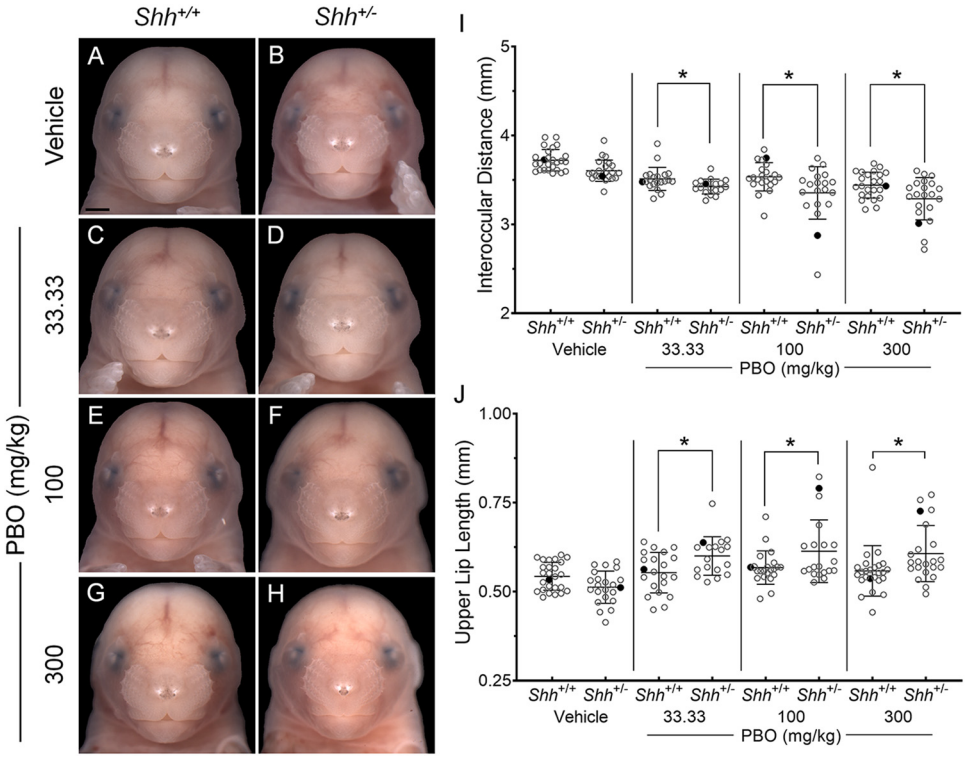

Figure 4. Evaluation of facial dysmorphology in PBO-exposed $Shh^{+/+}$ and $Shh^{+/-}$ fetuses. (A–H) $Shh^{+/+}$ and $Shh^{+/-}$ GD17 fetuses exposed to vehicle (olive oil) or indicated doses of PBO at GD7.75. (I,J) Interocular distance (IOD) and upper lip length (ULL) measurement for vehicle-exposed $Shh^{+/+}$ ($n=26$) and $Shh^{+/-}$ ($n=22$) fetuses, 33.33 mg/kg PBO-exposed $Shh^{+/+}$ ($n=21$) and $Shh^{+/-}$ ($n=18$), 100 mg/kg PBO-exposed $Shh^{+/+}$ ($n=22$) and $Shh^{+/-}$ ($n=20$), and 300 mg/kg PBO-exposed $Shh^{+/+}$ ($n=24$) and $Shh^{+/-}$ ($n=24$) fetuses. All individual data points are plotted along with bars representing the mean ± SD for each group. Filled circles in I and J indicate specific fetuses shown in A–H for the corresponding treatment group and genotype. One-way ANOVA with Tukey's post hoc test was used to compare the statistical significance of IOD and ULL measurements between genotype groups for each dose group. $^{*}p<0.05$. Scale bar: 1.0 mm. Note: ANOVA, analysis of variance GD, gestational day; PBO, piperonyl butoxide; SD, standard deviation; Shh, Sonic hedgehog.

GD7.75 in the mouse, equivalent to 3 weeks postconception in human development, disrupted development of the forebrain and face. The severity of PBO-induced outcomes was dose dependent and ranged from subtle to overt facial dysmorphology, corresponding with forebrain abnormalities that ranged from mild deficiency to the severe midline loss of full-blown HPE. Highlighting the potential for gene–environment interactions, we observed that the teratogenic effects of PBO were exacerbated by normally silent, single-allele *Shh* mutations that model common human HPE-associated mutations.

Unlike pyrethrin insecticides themselves, the potential developmental toxicity of PBO has received little attention. Previous examinations of PBO's teratogenic potential were untargeted and produced inconsistent results. A study of PBO exposure in pregnant rats published in 1952 reported that chronic dietary PBO administration adversely affected reproduction (Sarles and Vandegrift 1952). Two subsequent teratogenicity studies in rats were apparently negative, but high doses were reported to cause embryonic loss (Kennedy et al. 1977; Khera et al. 1979). In these studies, daily acute PBO exposure encompassed the critical period for HPE, but whether the phenotypic analysis was adequate to detect HPE-like phenotypes in surviving fetuses or offspring is unclear, and neither images nor craniofacial morphometric analyses were presented. A more recent examination of PBO teratogenicity in CD-1 mice found that a single maternal oral dose of PBO (as high as 1,065 or 1,800 mg/kg) administered at approximately GD9 resulted in forelimb digit reduction (Tanaka et al. 1994). Shh signaling is known to regulate limb development and digit patterning (Riddle et al. 1993), and the limb malformations observed following PBO exposure mimic outcomes we previously described in mice exposed to the potent Shh pathway inhibitor vismodegib at the same critical period of forelimb development (Heyne et al. 2015a). Although the study by Tanaka et al. (1994) did not examine the critical period for HPE (Heyne et al. 2015a), the finding that PBO resulted in phenotypically similar developmental limb abnormalities supports the hypothesis that *in utero* PBO exposure can cause structural malformations by inhibiting Shh signaling.

PBO was discovered as a Shh pathway inhibitor in a small molecule screening assay of over 1,400 toxicants (Wang et al. 2012). This original report found that PBO inhibited Shh signaling *in vitro* and was capable of competitively displacing radiolabeled cyclopamine, which inhibits the pathway by binding to the signal transducing protein SMO (Chen et al. 2002a). Here, we provide evidence suggesting that PBO inhibits Shh signaling *in vitro* in both mouse and human cells (Figure 1A–C). Consistent with acting directly on SMO, the results from our *in vitro* experiments suggest that PBO acts downstream of PTCH1 and upstream of GLI1 (Figure 1D–E) and that inhibition of Shh signaling transduction by PBO can be rescued by the addition of a SMO agonist (Figure 1F). Concentration–response comparisons suggested that PBO was approximately 4-fold less potent than cyclopamine, a plant alkaloid that was discovered as a teratogen causing HPE in the offspring of grazing sheep (Keeler 1978). PBO was found to be approximately 50-fold less potent than the highly potent and specific synthetic Shh pathway inhibitor vismodegib. We also found that exposure to vismodegib or PBO at the same time in development causes

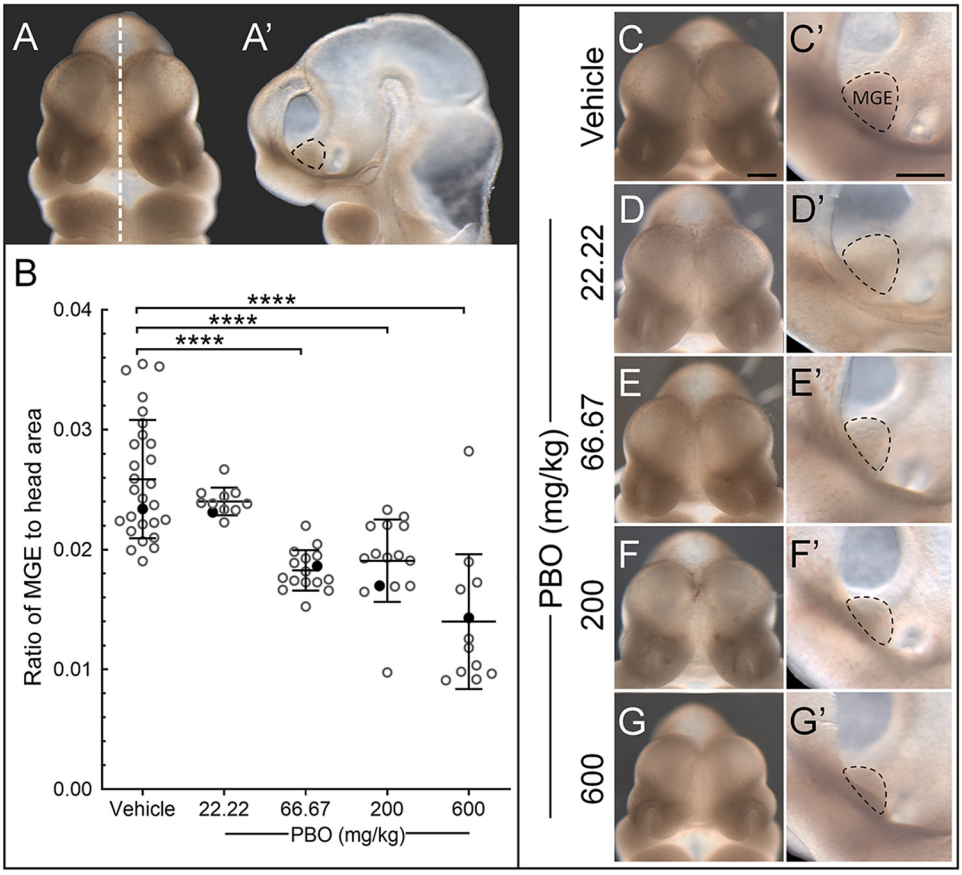

Figure 5. Evaluation of MGE morphology in PBO-exposed embryos. (A–A′) GD11 embryos exposed to vehicle (olive oil) or the indicated doses of PBO were hemisected at the sagittal midline (dashed line) to visualize the inside of the developing brain, including the MGE (dashed black outline in A′). (B) Quantification of MGE area normalized to head area. Measurements of all embryos collected from litters exposed to vehicle ($n=5$) or 22.22 ($n=3$), 66.67 ($n=3$), 200 ($n=3$), or 600 mg/kg PBO ($n=3$) are plotted along with bars representing the mean ± SD for each group. One-way ANOVA with Tukey's post hoc test was used to compare the statistical significance of normalized MGE measurements in PBO-exposed groups relative to the vehicle-exposed group. ****$p<0.0001$. Filled circles indicate the specific embryos shown in C–G and C′–G′. (C–G) Frontal images of GD11 embryos exposed to vehicle or the indicated dose of PBO at GD7.75. (C′–G′) Magnified images of hemisected embryos from C–G with the MGE indicated with the dashed black outline. Scale bars in C and C′: 0.25 mm. Note: ANOVA, analysis of variance; MGE, medial ganglionic eminence; PBO, piperonyl butoxide; GD, gestational day; SD, standard deviation.

comparable malformations of the brain and face (Figure 3; see also Figure S4).

Although gene–environment interactions are widely invoked to explain the complex etiology of human HPE, research efforts have primarily focused on the genetic side of this equation. *SHH* is among the most common genes associated with HPE (Nanni et al. 1999) but phenotypic outcomes are highly variable, such that even within a single family pedigree, some mutation carriers can be severely affected and others apparently normal (Solomon et al. 2012). In mice, homozygous *Shh* null mutations have been described to cause severe HPE (Chiang et al. 1996) while heterozygous *Shh* null animals appeared grossly indistinguishable from their WT siblings (Kietzman et al. 2014). Here, we found that *Shh* heterozygosity, although not resulting in detectable differences alone, exacerbated the teratogenic impact of PBO exposure (Figure 4). The implications of this specific gene–environment interaction may extend even more broadly, as most other mutations linked to HPE have been reported to be heterozygous and associated with wide phenotypic variability (Roessler and Muenke 2010). Efforts to elucidate the multifactorial etiology of HPE should also consider interactions between PBO and other HPE-associated environmental factors such as maternal diabetes (Johnson and Rasmussen 2010), alcohol consumption (Hong and Krauss 2017), and exposure to other environmental and dietary Shh signaling inhibitors (Elamin et al. 2010; Lipinski et al. 2007; Lipinski and Bushman 2010).

In both animal models (Heyne et al. 2016; Kietzman et al. 2014) and clinical cases (DeMyer et al. 1964; DeMyer 1971; El-Hawrani et al. 2006) of HPE, the degree of facial dysmorphology has been shown to predict the severity of co-occurring brain abnormalities. True HPE, defined by incomplete division of the cerebral cortices, causes profound intellectual disability and motor impairment (Weiss et al. 2018). We found that acute PBO exposure resulted in phenotypes consistent with true HPE, marked by severe median forebrain deficiency, hypotelorism, and midface hypoplasia, as illustrated by mice exposed to 1,800 mg/kg at GD7.75 (Figure 3). We also observed that lower doses of PBO (in addition to higher doses) caused more subtle disruptions of forebrain development, including abnormal morphogenesis of Shh-dependent MGEs (Figure 5). MGE-derived inhibitory gamma-aminobutyic acid–producing (GABAergic) cortical interneurons regulate multiple aspects of cognitive processing including emotion, self-control, learning, and memory (Le Magueresse and Monyer 2013). Dysfunction in these neurobehavioral domains has been linked to cortical interneuron deficiency in mouse genetic models and cortical interneuron imbalance is widely implicated in human neuropsychiatric disorders (Marín 2012). We have shown previously that perturbation of MGE development by transient Shh pathway

inhibition leads to sustained disruption of cortical interneuron migration and specification in the mouse (Ansen-Wilson et al. 2018). Patients with true HPE were found to exhibit a depletion of GABAergic cortical interneurons (Fertuzinhos et al. 2009), although the contribution of this particular deficit to the intellectual disability observed in such patient cohorts is unclear (Fertuzinhos et al. 2009).

The finding that PBO caused subtle forebrain abnormalities in the absence of overt facial dysmorphology may shed new light on human and animal model studies linking prenatal PBO exposure to neurobehavioral outcomes. An epidemiologic study found a significant inverse correlation between prenatal exposure to PBO and neurodevelopment in 36-month-old children (Horton et al. 2011). Interestingly, no correlation was found for exposure of the active pesticidal ingredient, suggesting an independent effect of PBO itself. Developmental exposure to PBO through maternal diet has also been shown to cause neurobehavioral deficits in mice. In these studies, the offspring of mice maintained on chow containing 0.01–0.09% PBO during gestation and lactation exhibited deficits in several tasks including exploratory and spontaneous behavior (Tanaka and Inomata 2015, 2016). To the best of our knowledge, neither human (Horton et al. 2011) nor animal (Tanaka and Inomata 2015, 2016) studies linking prenatal PBO exposure to neurobehavior deficits have examined a causative mechanism. The results reported here implicate disruption of Shh signaling as a plausible mechanism underlying the neurodevelopmental deficits linked to prenatal PBO exposure. Together, these findings support the premise that subteratogenic PBO exposure may result in subtle forebrain abnormalities in the absence of overt, easily recognizable facial dysmorphology.

Relative to active pesticidal components, the availability of empirical data informing our understanding of human exposure to PBO is limited. As a synergist, PBO is not included in the suite of pesticides examined in the National Health and Nutritional Examination Survey, and its developmental toxicity has not been assessed within the National Toxicology Program. In the present study, PBO was administered acutely to specifically target Shh signaling during the defined, narrow critical period for HPE. The environmental relevance of the doses that were found to impact brain and face development in mice is unclear because of the limited understanding of human PBO exposure and its pharmacokinetics in mice and humans. Administration by oral gavage was chosen because ingestion is likely a main exposure route of PBO. In addition to indoor dust, PBO consumption also occurs as food residue. PBO is used in food production and processing, including pre- and postharvest application on agricultural crops, treatment of livestock animals and premises, and treatment of commercial facilities where raw and processed food commodities are stored, processed, and prepared (U.S. EPA 2006). The recently emerging Zika health crisis portends increased PBO exposure to women of childbearing age given that insecticides containing PBO are among mosquito control products that may be used to prevent transmission of the Zika virus (U.S. EPA 2006). Because many PBO-containing products are applied as aerosol sprays or directly to the skin, human exposure to PBO likely also occurs through inhalation and dermal absorption. With reported logP values between 4.60 and 4.95 (U.S. EPA 2006; Tomlin and British Crop Protection Council 2000) PBO is lipophilic and may have the potential for bioaccumulation. However, to the best of our knowledge, the pharmacokinetics of PBO and its concentration range in human serum have not been rigorously examined.

In the present study, we provide evidence suggesting that the environmental toxicant PBO inhibits the Shh signaling pathway *in vitro* in mouse and human cells and that its targeted prenatal exposure in mice causes face and brain dysmorphology that is consistent with Shh pathway disruption and exacerbated by normally silent *Shh* mutations. By targeting a sensitive mechanism of action, this study defined an LOEL for PBO-induced developmental toxicity that is more than 30-fold lower than was previously recognized (U.S. EPA 2006; Tanaka et al. 1994). PBO exposure should be considered alongside other nongenetic HPE-associated factors, particularly in genetically sensitive populations. More broadly, these findings should prompt efforts to address major knowledge gaps in our understanding of human exposure to PBO and its potential role in the complex etiology of Shh signaling-related human birth defects and neurodevelopmental abnormalities.

Acknowledgments

The authors acknowledge the services of the University of Wisconsin-Madison Biotron Laboratory and the School of Pharmacy Mass Spectrometry Facility. The authors also thank A. Aylsworth, A. Steward, and K. Rivera-González for their critical review of the manuscript. Research reported in this publication was supported by the National Institute of Environmental Health Sciences of the National Institutes of Health (NIH) under award numbers R01ES026819 and T32ES007015. The content is solely the responsibility of the authors and does not necessarily represent the official views of the NIH.

References

Abler LL, Mehta V, Keil KP, Joshi PS, Flucus CL, Hardin HA, et al. 2011. A high throughput *in situ* hybridization method to characterize mRNA expression patterns in the fetal mouse lower urogenital tract. J Vis Exp 54:e2912, PMID: 21876526, https://doi.org/10.3791/2912.

Ansen-Wilson LJ, Everson JL, Fink DM, Kietzman HW, Sullivan R, Lipinski RJ. 2018. Common basis for orofacial clefting and cortical interneuronopathy. Transl Psychiatry 8(1):8, PMID: 29317601, https://doi.org/10.1038/s41398-017-0057-7.

Chen JK. 2016. I only have eye for ewe: the discovery of cyclopamine and development of Hedgehog pathway-targeting drugs. Nat Prod Rep 33(5):595–601, PMID: 2678t175, https://doi.org/10.1039/c5np00153f.

Chen JK, Taipale J, Cooper MK, Beachy PA. 2002a. Inhibition of Hedgehog signaling by direct binding of cyclopamine to Smoothened. Genes Dev 16(21):2743–2748, PMID: 12414725, https://doi.org/10.1101/gad.1025302.

Chen JK, Taipale J, Young KE, Maiti T, Beachy PA. 2002b. Small molecule modulation of Smoothened activity. Proc Natl Acad Sci USA 99(22):14071–14076, PMID: 12391318, https://doi.org/10.1073/pnas.182542899.

Chiang C, Litingtung Y, Lee E, Young KE, Corden JL, Westphal H, et al. 1996. Cyclopia and defective axial patterning in mice lacking *Sonic hedgehog* gene function. Nature 383(6599):407–413, PMID: 8837770, https://doi.org/10.1038/383407a0.

DeMyer W. 1971. Classification of cerebral malformations. Birth Defects Orig Artic Ser 7(1):78–93, PMID: 5173382.

DeMyer W, Zeman W, Palmer CG. 1964. The face predicts the brain: diagnostic significance of median facial anomalies for holoprosencephaly (arhinencephaly). Pediatrics 34:256–263, PMID: 14211086.

Elamin MH, Shinwari Z, Hendrayani SF, Al-Hindi H, Al-Shail E, Khafaga Y, et al. 2010. Curcumin inhibits the Sonic Hedgehog signaling pathway and triggers apoptosis in medulloblastoma cells. Mol Carcinog 49(3):302–314, PMID: 20025076, https://doi.org/10.1002/mc.20604.

El-Hawrani A, Sohn M, Noga M, El-Hakim H. 2006. The face does predict the brain—midline facial and forebrain defects uncovered during the investigation of nasal obstruction and rhinorrhea. Case report and a review of holoprosencephaly and its classifications. Int J Pediatr Otorhinolaryngol 70(5):935–940, PMID: 16280170, https://doi.org/10.1016/j.ijporl.2005.09.020.

Fertuzinhos S, Krsnik Ž, Kawasawa YI, Rašin M-R, Kwan KY, Chen J-G, et al. 2009. Selective depletion of molecularly defined cortical interneurons in human holoprosencephaly with severe striatal hypoplasia. Cereb Cortex 19(9):2196–2207, PMID: 19234067, https://doi.org/10.1093/cercor/bhp009.

Graham JM Jr, Shaw GM. 2005. Gene-environment interactions in rare diseases that include common birth defects. Birth Defects Res Part A Clin Mol Teratol 73(11):865–867, PMID: 16265646, https://doi.org/10.1002/bdra.20193.

Heyne GW, Everson JL, Ansen-Wilson LJ, Melberg CG, Fink DM, Parins KF, et al. 2016. *Gli2* gene-environment interactions contribute to the etiological complexity of holoprosencephaly: evidence from a mouse model. Dis Model Mech 9(11):1307–1315, PMID: 27585885, https://doi.org/10.1242/dmm.026328.

Heyne GW, Melberg CG, Doroodchi P, Parins KF, Kietzman HW, Everson JL, et al. 2015a. Definition of critical periods for Hedgehog pathway antagonist-induced holoprosencephaly, cleft lip, and cleft palate. PLoS One 10(3):e0120517, PMID: 25793997, https://doi.org/10.1371/journal.pone.0120517.

Heyne GW, Plisch EH, Melberg CG, Sandgren EP, Peter JA, Lipinski RJ. 2015b. A simple and reliable method for early pregnancy detection in inbred mice. J Am Assoc Lab Anim Sci 54(4):368–371, PMID: 26224435.

Hong M, Krauss RS. 2017. Ethanol itself is a holoprosencephaly-inducing teratogen. PLoS One 12(4):e0176440, PMID: 28441416, https://doi.org/10.1371/journal.pone.0176440.

Hong M, Krauss RS. 2018. Modeling the complex etiology of holoprosencephaly in mice. Am J Med Genet C Semin Med Genet 178(2):140–150, PMID: 29749693, https://doi.org/10.1002/ajmg.c.31611.

Horton MK, Rundle A, Camann DE, Boyd Barr D, Rauh VA, Whyatt RM. 2011. Impact of prenatal exposure to piperonyl butoxide and permethrin on 36-month neurodevelopment. Pediatrics 127(3):e699–e706, PMID: 21300677, https://doi.org/10.1542/peds.2010-0133.

Jacobsen PF, Jenkyn DJ, Papadimitriou JM. 1985. Establishment of a human medulloblastoma cell line and its heterotransplantation into nude mice. J Neuropathol Exp Neurol 44(5):472–485, PMID: 2993532, https://doi.org/10.1097/00005072-198509000-00003.

Johnson CY, Rasmussen SA. 2010. Non-genetic risk factors for holoprosencephaly. Am J Med Genet C Semin Med Genet 154C(1):73–85, PMID: 20104598, https://doi.org/10.1002/ajmg.c.30242.

Keeler RF. 1970. Teratogenic compounds of *Veratrum californicum* (Durand) X. Cyclopia in rabbits produced by cyclopamine. Teratology 3(2):175–180, PMID: 4986632, https://doi.org/10.1002/tera.1420030210.

Keeler RF. 1975. Teratogenic effects of cyclopamine and jervine in rats, mice and hamsters. Proc Soc Exp Biol Med 149(1):302–306, PMID: 1144444, https://doi.org/10.3181/00379727-149-38794.

Keeler RF. 1978. Cyclopamine and related steroidal alkaloid teratogens: their occurrence, structural relationship, and biologic effects. Lipids 13(10):708–715, PMID: 723484, https://doi.org/10.1007/bf02533750.

Kennedy GL Jr, Smith SH, Kinoshita FK, Keplinger ML, Calandra JC. 1977. Teratogenic evaluation of piperonyl butoxide in the rat. Food Cosmet Toxicol 15(4):337–339, PMID: 590894, https://doi.org/10.1016/s0015-6264(77)80207-1.

Khera KS, Whalen C, Angers G, Trivett G. 1979. Assessment of the teratogenic potential of piperonyl butoxide, biphenyl, and phosalone in the rat. Toxicol Appl Pharmacol 47(2):353–358, PMID: 452026, https://doi.org/10.1016/0041-008x(79)90330-2.

Kietzman HW, Everson JL, Sulik KK, Lipinski RJ. 2014. The teratogenic effects of prenatal ethanol exposure are exacerbated by Sonic Hedgehog or GLI2 haploinsufficiency in the mouse. PLoS One 9(2):e89448, PMID: 24586787, https://doi.org/10.1371/journal.pone.0089448.

Kohtz JD, Baker DP, Corte G, Fishell G. 1998. Regionalization within the mammalian telencephalon is mediated by changes in responsiveness to Sonic Hedgehog. Development 125(24):5079–5089, PMID: 9811591.

Krauss RS, Hong M. 2016. Gene–environment interactions and the etiology of birth defects. Curr Top Dev Biol 116:569–580, PMID: 26970642, https://doi.org/10.1016/bs.ctdb.2015.12.010.

Le Magueresse C, Monyer H. 2013. GABAergic interneurons shape the functional maturation of the cortex. Neuron 77(3):388–405, PMID: 23395369, https://doi.org/10.1016/j.neuron.2013.01.011.

Leoncini E, Baranello G, Orioli IM, Annerén G, Bakker M, Bianchi F, et al. 2008. Frequency of holoprosencephaly in the International Clearinghouse Birth Defects Surveillance Systems: searching for population variations. Birth Defects Res A Clin Mol Teratol 82(8):585–591, PMID: 18566978, https://doi.org/10.1002/bdra.20479.

Levey EB, Stashinko E, Clegg NJ, Delgado MR. 2010. Management of children with holoprosencephaly. Am J Med Genet C Semin Med Genet 154C(1):183–190, PMID: 20104615, https://doi.org/10.1002/ajmg.c.30254.

Lipinski RJ, Bijlsma MF, Gipp JJ, Podhaizer DJ, Bushman W. 2008. Establishment and characterization of immortalized Gli-null mouse embryonic fibroblast cell lines. BMC Cell Biol 9:49, PMID: 18789160, https://doi.org/10.1186/1471-2121-9-49.

Lipinski RJ, Bushman W. 2010. Identification of Hedgehog signaling inhibitors with relevant human exposure by small molecule screening. Toxicol In Vitro 24(5):1404–1409, PMID: 20434536, https://doi.org/10.1016/j.tiv.2010.04.011.

Lipinski RJ, Dengler E, Kiehn M, Peterson RE, Bushman W. 2007. Identification and characterization of several dietary alkaloids as weak inhibitors of Hedgehog signaling. Toxicol Sci 100(2):456–463, PMID: 17728282, https://doi.org/10.1093/toxsci/kfm222.

Lipinski RJ, Gipp JJ, Zhang J, Doles JD, Bushman W. 2006. Unique and complimentary activities of the Gli transcription factors in Hedgehog signaling. Exp Cell Res 312(11):1925–1938, PMID: 16571352, https://doi.org/10.1016/j.yexcr.2006.02.019.

Lipinski RJ, Godin EA, O'Leary-Moore SK, Parnell SE, Sulik KK. 2010. Genesis of teratogen-induced holoprosencephaly in mice. Am J Med Genet C Semin Med Genet 154C(1):29–42, PMID: 20104601, https://doi.org/10.1002/ajmg.c.30239.

Lipinski RJ, Hammond P, O'Leary-Moore SK, Ament JJ, Pecevich SJ, Jiang Y, et al. 2012. Ethanol-induced face-brain dysmorphology patterns are correlative and exposure-stage dependent. PLoS One 7(8):e43067, PMID: 22937012, https://doi.org/10.1371/journal.pone.0043067.

Lovely C, Rampersad M, Fernandes Y, Eberhart J. 2017. Gene–environment interactions in development and disease. Wiley Interdiscip Rev Dev Biol 6(1):e247, PMID: 27626243, https://doi.org/10.1002/wdev.247.

Marín O. 2012. Interneuron dysfunction in psychiatric disorders. Nat Rev Neurosci 13(2):107–120, PMID: 22251963, https://doi.org/10.1038/nrn3155.

Matsunaga E, Shiota K. 1977. Holoprosencephaly in human embryos: epidemiologic studies of 150 cases. Teratology 16(3):261–272, PMID: 594909, https://doi.org/10.1002/tera.1420160304.

Nanni L, Ming JE, Bocian M, Steinhaus K, Bianchi DW, Die-Smulders C, et al. 1999. The mutational spectrum of the *Sonic Hedgehog* gene in holoprosencephaly: SHH mutations cause a significant proportion of autosomal dominant holoprosencephaly. Hum Mol Genet 8(13):2479–2488, PMID: 10556296, https://doi.org/10.1093/hmg/8.13.2479.

NRC (National Research Council). 2011. *Guide for the Care and Use of Laboratory Animals*. Washington, DC: National Academies Press.

Petryk A, Graf D, Marcucio R. 2015. Holoprosencephaly: signaling interactions between the brain and the face, the environment and the genes, and the phenotypic variability in animal models and humans. Wiley Interdiscip Rev Dev Biol 4(1):17–32, PMID: 25339593, https://doi.org/10.1002/wdev.161.

Riddle RD, Johnson RL, Laufer E, Tabin C. 1993. *Sonic hedgehog* mediates the polarizing activity of the ZPA. Cell 75(7):1401–1416, PMID: 8269518, https://doi.org/10.1016/0092-8674(93)90626-2.

Robarge KD, Brunton SA, Castanedo GM, Cui Y, Dina MS, Goldsmith R, et al. 2009. GDC-0449-a potent inhibitor of the hedgehog pathway. Bioorg Med Chem Lett 19(19):5576–5581, PMID: 19716296, https://doi.org/10.1016/j.bmcl.2009.08.049.

Roessler E, Belloni E, Gaudenz K, Jay P, Berta P, Scherer SW, et al. 1996. Mutations in the human *Sonic Hedgehog* gene cause holoprosencephaly. Nat Genet 14(3):357–360, PMID: 8896572, https://doi.org/10.1038/ng1196-357.

Roessler E, Du YZ, Mullor JL, Casas E, Allen WP, Gillessen-Kaesbach G, et al. 2003. Loss-of-function mutations in the human *GLI2* gene are associated with pituitary anomalies and holoprosencephaly-like features. Proc Natl Acad Sci USA 100(23):13424–13429, PMID: 14581620, https://doi.org/10.1073/pnas.2235734100.

Roessler E, Hu P, Muenke M. 2018. Holoprosencephaly in the genomics era. Am J Med Genet C Semin Med Genet 178(2):165–174, PMID: 29770992, https://doi.org/10.1002/ajmg.c.31615.

Roessler E, Muenke M. 2010. The molecular genetics of holoprosencephaly. Am J Med Genet C Semin Med Genet 154C(1):52–61, PMID: 20104595, https://doi.org/10.1002/ajmg.c.30236.

Rudel RA, Camann DE, Spengler JD, Korn LR, Brody JG. 2003. Phthalates, alkylphenols, pesticides, polybrominated diphenyl ethers, and other endocrine-disrupting compounds in indoor air and dust. Environ Sci Technol 37(20):4543–4553, PMID: 14594359, https://doi.org/10.1021/es0264596.

Sarles MP, Vandegrift WB. 1952. Chronic oral toxicity and related studies on animals with the insecticide and pyrethrum synergist, piperonyl butoxide. Am J Trop Med Hyg 1(5):862–883, PMID: 14952712, https://doi.org/10.4269/ajtmh.1952.1.862.

Schneider CA, Rasband WS, Eliceiri KW. 2012. NIH Image to ImageJ: 25 years of image analysis. Nat Methods 9:671–675, PMID: 22930834, https://doi.org/10.1038/nmeth.2089.

Scott JG. 1996. Inhibitors of CYP6D1 in house fly microsomes. Insect Biochem Mol Biol 26(7):645–649, PMID: 8995787, https://doi.org/10.1016/S0965-1748(96)00008-2.

Solomon BD, Bear KA, Wyllie A, Keaton AA, Dubourg C, David V, et al. 2012. Genotypic and phenotypic analysis of 396 individuals with mutations in *Sonic Hedgehog*. J Med Genet 49(7):473–479, PMID: 22791840, https://doi.org/10.1136/jmedgenet-2012-101008.

Taipale J, Chen JK, Cooper MK, Wang B, Mann RK, Milenkovic L, et al. 2000. Effects of oncogenic mutations in *Smoothened* and *Patched* can be reversed by cyclopamine. Nature 406(6799):1005–1009, PMID: 10984056, https://doi.org/10.1038/35023008.

Taipale J, Cooper MK, Maiti T, Beachy PA. 2002. Patched acts catalytically to suppress the activity of Smoothened. Nature 418(6900):892–897, PMID: 12192414, https://doi.org/10.1038/nature00989.

Tanaka T, Fujitani T, Takahashi O, Oishi S. 1994. Developmental toxicity evaluation of piperonyl butoxide in CD-1 mice. Toxicol Lett 71(2):123–129, PMID: 8171442, https://doi.org/10.1016/0378-4274(94)90172-4.

Tanaka T, Inomata A. 2015. Effects of maternal exposure to piperonyl butoxide (PBO) on behavioral development in F_1-generation mice. Birth Defects Res B Dev Reprod Toxicol 104(6):227–237, PMID: 26431353, https://doi.org/10.1002/bdrb.21163.

Tanaka T, Inomata A. 2016. Reproductive and neurobehavioral effects of maternal exposure to piperonyl butoxide (PBO) in F_1-generation mice. Birth Defects Res B

Dev Reprod Toxicol 107(4–5):195–205, PMID: 27643382, https://doi.org/10.1002/bdrb.21185.

Theiler K. 1989. *The House Mouse: Atlas of Embryonic Development*. New York, NY: Springer-Verlag.

Tomlin C, British Crop Protection Council. 2000. *The Pesticide Manual: A World Compendium*. 12th ed. Farnham, UK: British Crop Protection Council.

U.S. EPA (U.S. Environmental Protection Agency). 2006. *Reregistration Eligibility Decision for Piperonyl Butoxide (PBO)*. EPA 738-R-06-005. Washington, DC: U.S. EPA, Office of Pesticide Programs.

Wang J, Lu J, Mook RA Jr, Zhang M, Zhao S, Barak L, et al. 2012. The insecticide synergist piperonyl butoxide inhibits Hedgehog signaling: assessing chemical risks. Toxicol Sci 128(2):517–523, PMID: 22552772, https://doi.org/10.1093/toxsci/kfs165.

Weiss K, Kruszka PS, Levey E, Muenke M. 2018. Holoprosencephaly from conception to adulthood. Am J Med Genet C Semin Med Genet 178(2):122–127, PMID: 30182446, https://doi.org/10.1002/ajmg.c.31624.

Xu Q, Wonders CP, Anderson SA. 2005. Sonic hedgehog maintains the identity of cortical interneuron progenitors in the ventral telencephalon. Development 132(22):4987–4998, PMID: 16221724, https://doi.org/10.1242/dev.02090.